TRANSIENT THERMOELASTIC CONTACT AND STABILITY OF TWO THIN-WALLED CYLINDERS

Ronggang Zhang
J. R. Barber
Department of Mechanical Engineering and Applied Mechanics
University of Michigan
Ann Arbor, Michigan 48109-2125

A solution is given for the problem of two thin-walled making contact at their plane end faces and transmitting a heat flux in the axial direction. It is assumed that a pressure-dependent thermal contact resistance exists at the interface. The problem has a trivial one-dimensional steady-state solution, which however is known to be unstable for certain material combinations if the heat flux is sufficiently large. The transient behavior is investigated here by representing the thermal and elastic fields by Fourier series in the circumferential and Fourier transforms in the axial direction. The results show that under certain circumstances a disturbance of constant form can move around the interface circumferentially.

INTRODUCTION

When heat is conducted across an interface between two contacting bodies, thermoelastic distortion influences the contact pressure distribution and sometimes the extent of the contact region. This in turn affects the boundary conditions for the heat conduction problem, particularly if, as is generally the case, there exists a pressure-dependent thermal contact resistance at the interface. The thermal and elastic problems are therefore fully coupled through the boundary conditions at the interface.

As a result of this coupling, steady-state solutions to the problem may be nonunique and/or unstable. Uniqueness and existence of steady-state solutions have been considered by Duvaut [1] and Shi and Shillor [2] using functional analysis techniques. The earliest investigations of thermoelastic contact stability [3–5] were restricted to one-dimensional systems such as a rod contacting a rigid wall [3] or axisymmetric concentric cylinders of similar materials [5]. For these systems, conditions can be found for which the steady state is unique, in which case it is always stable. Under other conditions, however, multiple steady-state solutions are found, some of which are stable and others unstable. In such cases, we anticipate that whatever initial condition is chosen for the system, it will eventually gravitate to one of the stable steady states.

The first author is now at Delco Electronics, Mail Station 6044, Kokomo, Indiana 46902.

J. R. Barber is pleased to acknowledge support from the National Science Foundation under Contract number MSM-8820623.

Journal of Thermal Stresses, 16:31–54, 1993

0149-5739/93 $10.00 + .00

Barber and Zhang [6] investigated the more complex one-dimensional system of two contacting rods of dissimilar materials and found that in this case steady-state solutions can be unstable even when they are unique. They also developed a numerical solution for the transient behavior and found that in such cases a nonlinear oscillatory behavior was developed, with alternating periods of contact and separation between the rods.

The simplest two-dimensional problem is that of two elastic half-planes in contact at a common interface. This system has a simple one-dimensional steady state in which the contact pressure at the interface is uniform and there is uniform heat flux normal to the interface, with a temperature jump at the interface associated with the thermal contact resistance. Barber [7] adapted the methods of Dow and Burton [8] and Richmond and Huang [9] for related problems to examine the stability of this solution by linear perturbation methods. The assumed perturbation involved a sinusoidal variation in temperature and stress in the direction parallel to the interface. As in the one-dimensional case, uniqueness and stability criteria were found to coincide when one of the materials was taken to be rigid, but when both half-planes were assumed to be deformable, cases could be found for which the steady state could be unique but unstable. In a subsequent investigation [10], it was shown that the stability criterion depended on the values of three dimensionless ratios of the bimaterial properties and that a substantial number of practical material combinations would exhibit this more complex behavior.

The purpose of the present article is to develop a numerical simulation to investigate the nonlinear transient behavior of such a system, in particular with a view to determining what kind of state it can support under conditions where the only steady-state configuration is unstable.

PROBLEM STATEMENT

We consider the problem of two thin-walled cylinders of radius r, wall thickness d, occupying the regions $y > 0$, $y < 0$ respectively and making contact at their common end plane $y = 0$ as shown in Figure 1. The cylinders are pressed together by a force P at the extremities and initially transmit a uniform heat flux $q_y = q_0$ in the positive y-direction. The two cylinders are of different materials, the appropriate material properties being distinguished by the suffix 1 for the cylinder $y > 0$ and 2 for $y < 0$. We suppose that there exists a thermal contact resistance R at the interface, which is a function of the local contact pressure or gap. For the purpose of the present simulation, we use an algorithm developed in [7], based on the experimental data of Thomas and Probert [11] for an interface between stainless steel and aluminum.

If shell bending effects can be neglected, this system can be unwrapped to give a plane stress problem for two contacting half-planes, with the restriction that the solution be periodic in x with period $2\pi r$. The range of parameters under which this approximation is legitimate is discussed in a similar isothermal problem by Azarkhin and Barber [12].

First, we characterize the temperature fields and present the updating algorithm; expressions for the corresponding thermoelastic displacements are then developed; and, finally, the algorithm for the solution of the contact problem is described.

The Heat Conduction Solution

We express the temperature field in the form of a Fourier series in x, i.e.,

$$T(x, y, t) = \sum_{i=0}^{N} F_i(y, t) \cos(m_i x) + \sum_{i=1}^{N} G_i(y, t) \sin(m_i x) \tag{1}$$

where $m_i = i/r$. The term $F_0(y, t)$ will require special attention, since it describes the initial linear temperature distribution in the body and hence does not decay as $y \to 0$. We shall return to it when we consider the case $i = 0$ and meanwhile concentrate on the remaining terms for which $i \neq 0$.

Suppose that the temperature field and the heat flux $q_y(x, 0)$ at the interface are known at some time t, which we can define as $t = 0$ without loss of generality. We wish to determine the temperature field after some small time increment δt, during which the heat flux is assumed to be constant. We write the temperature field during this time increment as the sum of two parts:

$$T(x, y, t) = T_s(x, y) + T_t(x, y, t) \tag{2}$$

where T_s is the steady-state temperature field that satisfies the boundary condition

$$\frac{\partial T_s}{\partial y}(x, 0) = -\frac{q_y(x, 0)}{K} \tag{3}$$

and K is the conductivity of the body.

The second term, $T_t = T - T_s$, in Eq. (2) must therefore satisfy the condition

$$\frac{\partial T_t}{\partial y}(x, 0, t) = 0 \tag{4}$$

Both terms must also satisfy the heat conduction equation

$$\nabla^2 T = \frac{1}{k} \frac{\partial T}{\partial t} \tag{5}$$

where k is the thermal diffusivity. The appropriate Fourier form for T_s is

$$T_s(x, y) = \sum_{i=1}^{N} e^{-m_i y}[C_i \cos(m_i x) + D_i \sin(m_i x)] \tag{6}$$

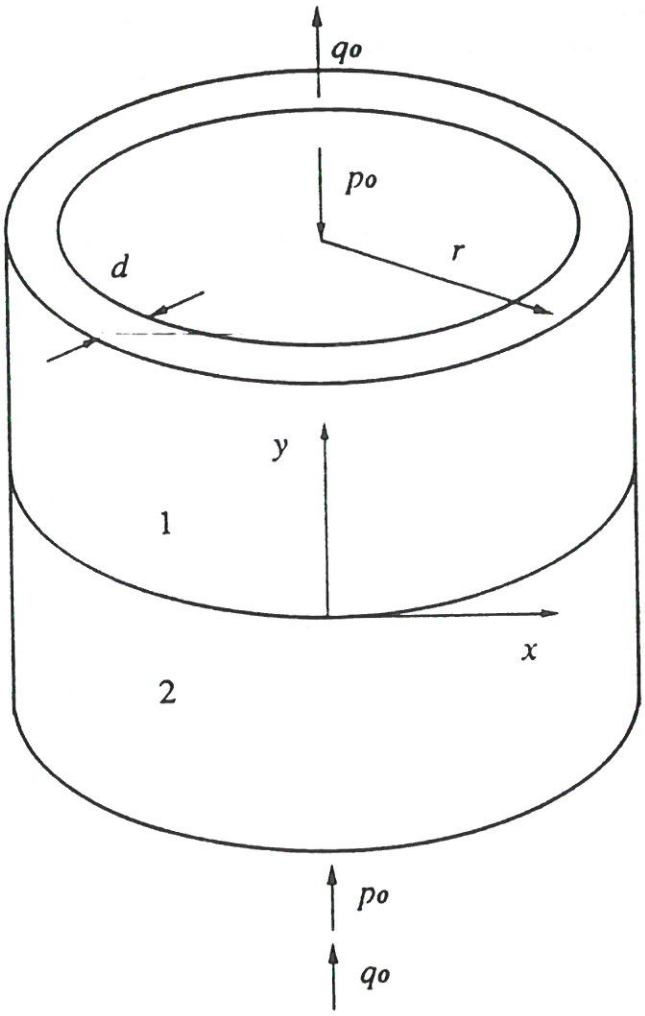

Fig. 1 Two thin-walled cylinders in contact on an end face.

SOLUTION METHOD

The coupled nature and the complexity of this problem necessitates a numerical approach. We use an explicit time-marching algorithm. The temperature field at any time t is expressed in terms of a Fourier series in x and a Fourier transform in y. This description permits us to calculate the unrestricted thermal distortion of the cylinders at time t, which then define the initial surface profiles for a thermoelastic contact problem. We then solve the contact problem numerically to determine the contact pressure or gap as a function of x and hence compute the instantaneous local contact resistance using the same algorithm as in [7]. Finally, we calculate the instantaneous heat flux $q_y(x, 0, t)$ at the interface from the local contact resistance and temperature difference and use the result to update the temperature field for the next time step $(t + \delta t)$. The whole process is then repeated to trace the long-term behavior of the system.

The above steps in the numerical solution are discussed in separate sections.

where C_i, D_i are unknown constants to be determined from the boundary condition (3). A suitable representation for T_t is

$$T_t(x, y, t) = \sum_{i=1}^{N} \int_0^{\infty} [A_i(n) \cos(m_i x) + B_i \sin(m_i x)] e^{-k(m_i^2+n^2)t} \cos(ny)\, dn \qquad (7)$$

where the choice of the cosine transform ensures that the boundary condition (4) is satisfied identically and $A_i(n)$, $B_i(n)$ are unknown functions to be determined from the initial condition $T(x, y, 0)$.

The case $i = 0$. When $i = 0$, the steady-state solution T_s reduces to the linear form

$$T_s(x, y) = C_0 + D_0 y \qquad (8)$$

Notice that in contrast to the Fourier terms of Eq. (6), this expression does not decay as $y \to \infty$. It follows that the corresponding term in T_t will not generally tend to zero as $y \to \infty$ and hence cannot be represented by a Fourier integral of the form (7). We therefore have to use a different representation, which will be developed in the present section.

The temperature field will be assumed to start from a small perturbation on a state of uniform conduction.* As the process develops, the uniform term in the heat flux will generally change, but, for finite t, the asymptotic temperature field at large y will be unaffected. A "boundary layer" will be developed near $y = 0$ in which the temperature field deviates from Eq. (8) and the thickness of this layer will increase with time, but the perturbation will always decay to zero as $y \to \infty$.

A suitable modification of the representation for $i \neq 0$ is to write the term for $i = 0$ in the form

$$T(y, t) = C_0 + D_0 y + T_1(y, t) + T_2(y, t) \qquad (9)$$

where

$$T_1(y, 0) = 0 \qquad \frac{\partial T_1}{\partial y}(0, t) + D_0 = -\frac{q}{K} \qquad (10)$$

the constants C_0, D_0 are chosen to describe the linear asymptotic form of the temperature field as $y \to \infty$ (and hence will remain unchanged throughout any finite time evolution of the process) and q is the zeroth term in a Fourier expansion of $q_y(x, 0)$.

*Even if some more general initial condition is assumed, the same argument can be applied, provided that the initial temperature field has a linear asymptotic form as $y \to \infty$.

These conditions completely define the term T_1, which can be evaluated in closed form as

$$T_1(y, t) = \left(\frac{q}{K} + D_0\right) F(y, t) \tag{11}$$

where

$$F(y, t) = 2\sqrt{\frac{kt}{\pi}} \exp\left(-\frac{y^2}{4kt}\right) - y \operatorname{erfc}\left(\frac{y}{2\sqrt{kt}}\right) \tag{12}$$

(see [13, §2.9]).

Since the term T_1 accounts for the heat flux at $y = 0$, we have

$$\frac{\partial T_2}{\partial y}(0, t) = 0 \tag{13}$$

and the initial value of T_2 is determined from $T(y, 0)$ by substituting Eq. (11) into Eq. (9). Furthermore, since the asymptotic behavior of the temperature field at large y is described by the linear terms $C_0 + D_0 y$, we conclude that $T_2(y, t) \to 0$ as $y \to \infty$ and therefore is conveniently represented in the Fourier integral form

$$T_2(y, t) = \int_0^\infty A_0(n) e^{-kn^2 t} \cos(ny)\, dn \tag{14}$$

This expression satisfies the heat conduction equation (5) and the boundary condition (12) for all values of the arbitrary function $A_0(n)$, which can therefore be used to satisfy the initial condition $T_2(y, 0)$.

Updating algorithm. The above expressions can be combined to give a representation for the complete temperature field during a given time increment in the form

$$\begin{aligned} T(x, y, t) = C_0 + D_0 y + \left(\frac{q}{K} + D_0\right) F(y, t) + \int_0^\infty A_0(n) e^{-kn^2 t} \cos(ny)\, dn \\ + \sum_{i=1}^{N} e^{-m_i y}[C_i \cos(m_i x) + D_i \sin(m_i x)] \cos(ny)\, dn \\ + \sum_{i=1}^{N} \int_0^\infty [A_i(n) \cos(m_i x) + B_i \sin(m_i x)] e^{-k(m_i^2 + n^2)t}\, dn \end{aligned} \tag{15}$$

Also, the heat flux at the interface is

$$q_y(x, 0) = -K \frac{\partial T}{\partial y}(x, 0) = q + K \sum_{i=1}^{N} m_i [C_i \cos(m_i x) + D_i \sin(m_i x)] \tag{16}$$

At the end of the time increment $t = \delta t$, a new expression is calculated for the heat flux $q_y(x, 0)$ based on the new values of the temperatures at the interface $T(x, 0, \delta t)$ and the thermal contact resistance. This expression is used to determine new values of the constants q, C_i, D_i in Eq. (15).

The remaining parameters are then updated by demanding that the temperature at the end of the current time step should be equal to that at the start of the next time step, i.e.,

$$T^-(x, y, \delta t) = T^+(x, y, 0) \tag{17}$$

where $-$ and $+$ refer to the current time step and the next time step respectively.

Substituting for the temperature field from Eq. (14) and equating coefficients of the Fourier terms, we obtain

$$\int_0^\infty A_0^-(n)e^{-kn^2\delta t}\cos(ny)\,dn + \left(\frac{q^-}{K} + D_0\right)F(y, \delta t)$$

$$= \int_0^\infty A_0^+(n)\cos(ny)\,dn + \left(\frac{q^+}{K} + D_0\right)F(y, 0) \tag{18}$$

$$\int_0^\infty A_i^-(n)e^{-k(m_i^2+n^2)\delta t}\cos(ny)\,dn + C_i^-e^{-m_i y}$$

$$= \int_0^\infty A_i^+(n)\cos(ny)\,dn + C_i^+e^{-m_i y} \tag{19}$$

$$\int_0^\infty B_i^-(n)e^{-k(m_i^2+n^2)\delta t}\cos(ny)\,dn + D_i^-e^{-m_i y}$$

$$= \int_0^\infty B_i^+(n)\cos(ny)\,dn + D_i^+e^{-m_i y} \tag{20}$$

These relations can be simplified by inverting the Fourier transforms and performing the resulting integrals, with the result

$$A_0^+(n) = A_0^-(n)e^{-kn^2\delta t} + \frac{2}{\pi n^2}\left(\frac{q^-}{K} + D_0\right)(1 - e^{-kn^2\delta t}) \tag{21}$$

$$A_i^+(n) = A_i^-e^{-k(m_i^2+n^2)\delta t} + \frac{2m_i(C_i^- - C_i^+)}{\pi(m_i^2 + n^2)} \tag{22}$$

$$B_i^+(n) = B_i^-e^{-k(m_i^2+n^2)\delta t} + \frac{2m_i(D_i^- - D_i^+)}{\pi(m_i^2 + n^2)} \tag{23}$$

which constitute a set of recurrence relations for the updated values of the functions $A_i(n)$, $B_i(n)$.

When $n = 0$, Eq. (21) is indeterminate, but the appropriate relation can be obtained by a limiting process, with the result

$$A_0^+(n) = A_0^-(n) + \frac{2k\delta t}{\pi}\left(\frac{q^-}{K} + D_0\right) \tag{24}$$

This expression can also be used for very small but finite values of $kn^2\delta t$, for which direct evaluation of Eq. (21) would lead to truncation errors.

Unrestrained Thermoelastic Distortion

We next determine the distortion of the surface $y = 0$, which would be produced by the temperature field (15), if the surface were free of tractions; i.e.,

$$\sigma_{yy}(x, 0) = \sigma_{yx}(x, 0) = 0 \tag{25}$$

We note that those terms in Eq. (15) that are independent of x will produce only a uniform displacement of the surface plane, which will have no effect on the contact pressure distribution. We can therefore restrict attention to the Fourier terms with $i \neq 0$.

The thermoelastic solution can be constructed as the sum of a particular thermoelastic solution and a homogeneous (isothermal) solution, the latter containing sufficient generality to permit the boundary conditions (25) to be satisfied.

The particular solution. The particular solution is conveniently expressed in terms of a thermoelastic displacement potential ψ, which is required to satisfy the governing equation [14]

$$\nabla^2\psi = \alpha(1 + \nu)T(x, y) \tag{26}$$

for plane stress, where α, ν are respectively the coefficient of thermal expansion and Poisson's ratio for the material. The important displacement and stress components are then given by

$$u_y = \frac{\partial\psi}{\partial y} \qquad \sigma_{yx} = \frac{E}{(1 + \nu)}\frac{\partial^2\psi}{\partial x\partial y} \qquad \sigma_{yy} = -\frac{E}{(1 + \nu)}\frac{\partial^2\psi}{\partial x^2} \tag{27}$$

where E is Young's modulus.

A suitable potential satisfying Eq. (26), with $T(x, y)$ given by the x-varying terms in Eq. (15) is

$$\psi = -\sum_{i=1}^{N}\frac{\alpha(1 + \nu)}{2m_i} ye^{-m_i y}[C_i\cos(m_i x) + D_i\sin(m_i x)]$$

$$-\sum_{i=1}^{N}\int_0^\infty \frac{\alpha(1 + \nu)m_i^2}{m_i^2 + n^2}[A_i(n)\cos(m_i x) + B_i(n)\sin(m_i x)]$$

$$\times \cos(ny)e^{-k(m_i^2 + n^2)t}\, dn \tag{28}$$

The corresponding traction and displacement components at the surface are

$$u_y(x, 0) = -\frac{\alpha(1+\nu)}{2}\sum_{i=1}^{N}\frac{1}{m_i}[C_i\cos(m_i x) + D_i\sin(m_i x)] \tag{29}$$

$$\sigma_{yx}(x, 0) = -\frac{E\alpha}{2}\sum_{i=1}^{N}[-C_i\sin(m_i x) + D_i\cos(m_i x)] \tag{30}$$

$$\sigma_{yy}(x, 0) = -E\alpha\sum_{i=1}^{N}\int_0^{\infty}\frac{m_i^2}{m_i^2+n^2}[A_i(n)\cos(m_i x) + B_i(n)\sin(m_i x)]e^{-k(m_i^2+n^2)t}\,dn \tag{31}$$

from Eqs. (27) and (28).

The isothermal solution. In order to satisfy the boundary conditions (25), it is necessary to superpose a solution of the corresponding isothermal problem on the particular thermoelastic solution of the previous section. The isothermal solution is conveniently defined in terms of the Airy stress function ϕ, a suitable biharmonic form being

$$\phi(x, y) = \sum_{i=1}^{N} e^{-m_i y}[(P_i + yQ_i)\cos(m_i x) + (R_i + yS_i)\sin(m_i x)] \tag{32}$$

The traction components at the surface are then given by

$$\sigma_{yx}(x, 0) = -\frac{\partial^2\phi}{\partial x\partial y}(x, 0)$$

$$= \sum_{i=1}^{N} m_i[-(m_i P_i - Q_i)\sin(m_i x) + (m_i R_i - S_i)\cos(m_i x)] \tag{33}$$

$$\sigma_{yy}(x, 0) = \frac{\partial^2\phi}{\partial x^2}(x, 0) = \sum_{i=1}^{N} m_i^2[P_i\cos(m_i x) + R_i\sin(m_i x)] \tag{34}$$

Superposing these tractions on those from the particular solution [Eqs. (30) and (31)] and substituting into the boundary conditions (16), we obtain four sets of algebraic equations for the unknown constants P_i, Q_i, R_i, S_i, with solution

$$P_i = -E\alpha\int_0^{\infty}\frac{e^{-k(m_i^2+n^2)t}}{(m_i^2+n^2)}A_i(n)\,dn \tag{35}$$

$$Q_i = m_i P_i - \frac{E\alpha}{2m_i}C_i \tag{36}$$

$$R_i = -E\alpha \int_0^\infty \frac{e^{-k(m_i^2+n^2)t}}{(m_i^2 + n^2)} B_i(n)\, dn \tag{37}$$

$$S_i = m_i R_i + \frac{E\alpha}{2m_i} D_i \tag{38}$$

The displacement field associated with the isothermal solution can now be found by substituting these constants into Eq. (32) for ϕ, calculating the complete isothermal stress field from the Airy stress function definitions, using the plane stress Hooke's law to find the strain components and integrating the strains to obtain the displacements. The procedure is lengthy but routine.

Superposing the resulting expression for the normal surface displacement on that from the particular solution (29), we obtain

$$u^t \equiv u_y(x, 0) = -\alpha \sum_{i=1}^{N} \left[\left(\frac{C_i}{m_i} + 2 \int_0^\infty \frac{m_i e^{-k(m_i^2+n^2)t}}{(m_i^2 + n^2)} A_i(n)\, dn \right) \cos(m_i x) \right.$$

$$\left. + \left(\frac{D_i}{m_i} + 2 \int_0^\infty \frac{m_i e^{-k(m_i^2+n^2)t}}{(m_i^2 + n^2)} B_i(n)\, dn \right) \sin(m_i x) \right] \tag{39}$$

which defines the shape of the unrestrained surface due to thermal distortion.

The Contact Problem

Equation (39) defines the distorted shape of the traction-free plane end of a cylinder, whose temperature is given by Eq. (15). The distortion of each of the two contacting cylinders will be described by an equation of this form, and we shall denote the corresponding displacements by u_1^t, u_2^t respectively.

When the two cylinders are pressed together, contact tractions $p(x) \equiv -\sigma_{yy}(x, 0)$ will be developed, which will produce additional normal surface displacements u_1^c, u_2^c. These two effects will cause a gap at the interface defined by

$$g(x) = [u_1^t(x) - u_2^t(x)] + [u_1^c(x) - u_2^c(x)] - C \tag{40}$$

where C defines a rigid body displacement. Notice that this equation could be generalized to the case where the undistorted ends of the cylinders were not plane (and hence nonconforming) by including an additional term $g_0(x)$ describing the initial gap between the undistorted surfaces.

The interface must contain a contact region A, in which the gap $g(x)$ is zero and the contact traction compressive, and it may also contain a separation region $\bar{A}$ in which the contact traction is zero and the gap positive; i.e.,

$$g(x) = 0 \quad p(x) > 0 \qquad x \in A \tag{41}$$

$$p(x) = 0 \quad g(x) > 0 \qquad x \in \bar{A} \tag{42}$$

To conform with the Fourier series representation of the preceeding sections, we represent the contact pressure distribution in the form

$$p(x) = p_0 + \sum_{i=1}^{N} [p_i^c \cos(m_i x) + p_i^s \sin(m_i x)] \tag{43}$$

Notice that the first term in this series can be found immediately from equilibrium considerations, being given by

$$p_0 = \frac{P}{2\pi r \delta} \tag{44}$$

(see Fig. 1).

The normal surface displacement due to this traction can be written down by superposition, using the plane stress equivalents of Johnson [15, §13.2], as

$$u_j^c = \frac{2}{E_j} \sum_{i=1}^{N} \frac{1}{m_i} [p_i^c \cos(m_i x) + p_i^s \sin(m_i x)] \tag{45}$$

where E_j, $j = 1, 2$ denotes the Young's modulus of materials 1, 2 respectively and we have omitted an indeterminate constant describing a rigid body displacement.

Solution algorithm. The extent of the contact region A is not known a priori and is determined from the unilateral inequalities in Eqs. (41) and (42). In the numerical algorithm, this necessitates an iterative solution. We define $(2N + 1)$ equally spaced points around the circumference at the interface and make an initial guess as to which points are in contact and which separated.

One equation is obtained for each contact point by substituting for u_j^c, u_j^I from Eqs. (45) and (39) respectively into Eqs. (40) and (41) and one for each separation point by substituting Eq. (43) into Eq. (42), giving a set of $(2N + 1)$ linear equations for the $2N$ coefficients p_i^c, p_i^s and the constant C. These equations are then solved and the appropriate inequalities in Eqs. (41) and (42) are checked to see whether the assumed division into contact and separation points was correct. At any point where the inequality is violated, the assumed status is changed and the solution repeated until convergence is obtained, which usually requires only a few iterations.

NUMERICAL ACCURACY AND CONVERGENCE

In a numerical simulation of such complexity, it is very difficult to assess the accuracy of the results or to identify potential sources of numerical instability. For this reason, each of the separate algorithms described above was first tested exhaustively against appropriate analytical solutions. For example, the algorithm for solving the contact problem was tested using the isothermal problem of contact between two sinusoidal surfaces, which exhibits periodic regions of contact and separation at suf-

ficiently small applied loads. A closed form solution of this problem is given by Westergaard [16] (see also [15]). The numerical algorithm gave very good accuracy, except in the immediate vicinity of the edge of the contact zone.

The heat conduction algorithm was tested against a variety of analytical solutions with prescribed thermal boundary conditions at the interface. Some of these were taken from Carslaw and Jaeger [13], and others were solved specifically for this purpose using standard methods.

In all time-marching algorithms, great care must be exercised in choosing the time step, since too great a time step will lead to inaccuracy and, in the case of explicit schemes, to instability. Difficulty can also be encountered if the time step is too small, since proportional changes in some physical quantities may be smaller than the numerical precision of their representation, leading to convergence on a spurious steady state.

Some guidance as to the appropriate time step can be obtained from the parameter $M = k\delta t/\epsilon^2$, where ϵ is a representative measure of the spatial discretization. In the present algorithm, we might associate ϵ with the wave length of the highest order Fourier term or with the smallest interval used in the inversion of the Fourier integral, whichever is the smallest. In finite difference algorithms, M is required to be less than 0.5 for stability. In the present simulation, M was reduced from 0.5 until further reduction gave no significant change in the predicted evolution of the system. Typical values of M to achieve this were in the range 0.006 to 0.01.

RESULTS

We consider cases in which the two cylinders are of aluminum alloy and stainless steel respectively, since experimental data for the pressure dependence of thermal contact resistance is available for this material combination [6, 11], being summarized in Figure 6 of [6]. The corresponding material properties used are given in Table 1 of [6]. In the classification of reference [12], this is a type 2 material combination, for which instability can be obtained for sufficiently large heat flux in either direction, the stability boundaries being defined by Figure 3 of [12].

Small Perturbations

We anticipate that the behavior of the system should follow that described by the linear analysis [11, 12] as long as the perturbation on the steady-state with uniform pressure and heat conduction is sufficiently small. We can therefore use the results of this analysis to test the satisfactory operation of the simulation algorithm as a whole.

Initial conditions. When the steady state is unstable, growth of the dominant eigenfunction of the stability analysis should be triggered by any initial perturbation. It is convenient, however, to test the algorithm by choosing parameters such as to make the longest wave length Fourier term have a positive growth rate and using an initial condition in which this term is given a small initial value.

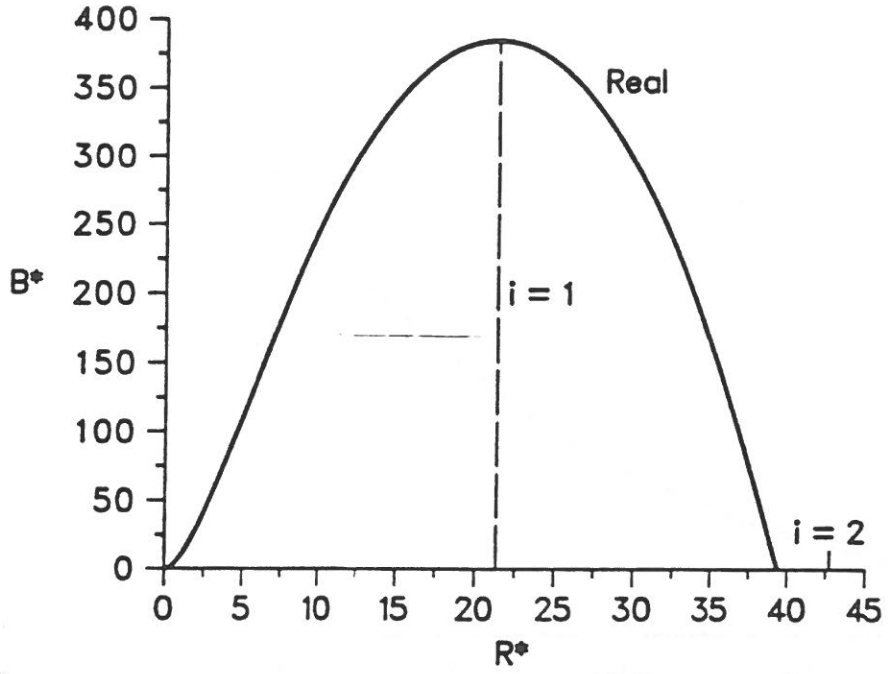

Fig. 2 Dimensionless growth rate of a disturbance for $Q^* = 100$.

Real roots. The simplest behavior is associated with the case where the heat flow is directed into the stainless steel body, in which case the analysis of [12] predicts that all unstable sinusoidal perturbations have real exponential growth rates. The exponential growth rate b can be characterized by a relation between dimensionless growth rate B^*, heat flux Q^*, and spatial frequency R^*, where

$$B^* \equiv \frac{(R_0K_1)^2b}{k_1} \qquad Q^* \equiv \frac{-2E_1E_2R'\alpha_1q_0}{E_1 + E_2} \qquad R^* \equiv R_0K_1m_i \tag{46}$$

and $R' = \partial R/\partial p$ is the derivative of the contact resistance with respect to pressure at the steady-state pressure p_0, at which the resistance is R_0. For more details of the relations between these quantities, the reader is referred to [12].

Figure 2 shows the dimensionless growth rate for $Q^* = 100$. The parameter values were chosen so as to make the first wave ($i = 1$) occur near the maximum growth rate. With this choice, all the higher wave numbers ($i > 1$) have negative growth rates and are therefore stable. Figure 3 shows the growth of the Fourier cosine coefficient p_1^c, which was given an initial perturbation. The growth is monotonic and initially exponential with a growth rate close to that predicted by the perturbation analysis. None of the higher pressure coefficients were observed to grow to significant values.

Complex roots. For the opposite direction of heat flow—into the aluminium alloy body—we anticipate perturbations with complex as well as real growth rates. Figure 4 shows the real part of the dimensionless growth rate for $Q^* = -200$. This corresponds to a point below the line R in Figure 2 of [12], and we therefore find a

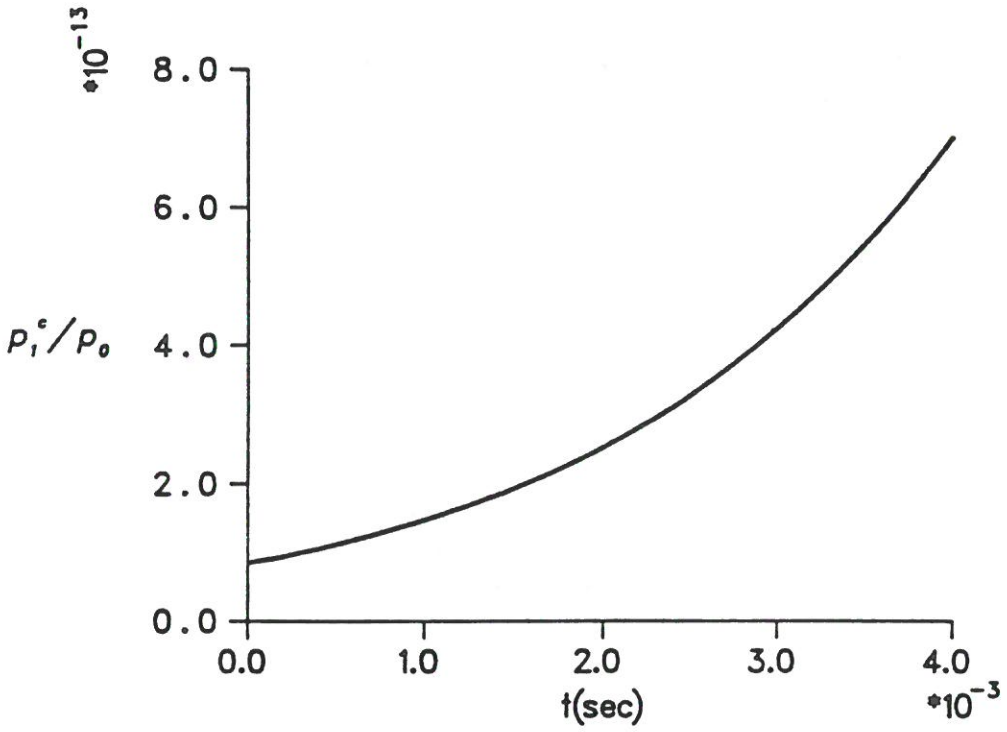

Fig. 3 Growth of the coefficient p_1^c for $Q^* = 100$.

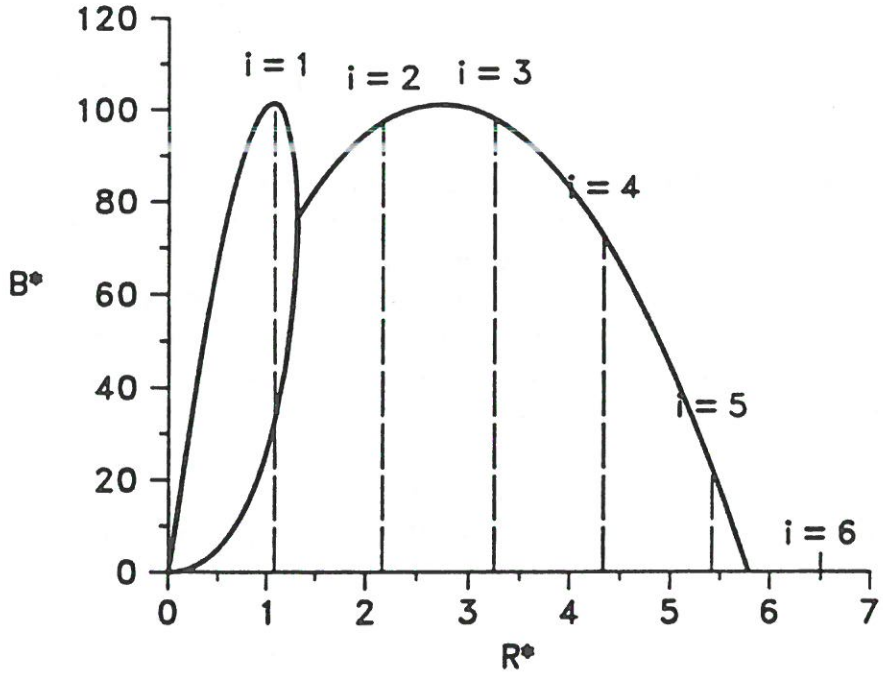

Fig. 4 Dimensionless growth rate of a disturbance for $Q^* = -200$. The two curves in the range $0 < R^* < 1.2$ correspond to real growth rates, whereas, in $R^* > 1.2$, B^* is the real part of a complex growth rate.

range of wave lengths with real growth rates and a contiguous range with complex growth rates. The parameter values were chosen so as to make the first wave (i = 1) occur near the maximum growth rate in the real range. With this choice, the wave numbers $i = 2, \ldots, 5$ fall into the complex range with positive growth rate, while higher wave numbers ($i > 6$) have negative growth rates and are therefore stable.

Figures 5 and 6 show the growth of the Fourier cosine coefficients p_i^c for $i = 1, \ldots, 5$. The system is initially dominated by the first wave number on which the perturbation was imposed, but the coefficients for $i = 2, \ldots, 5$ start to grow after an initial period. Notice that the growth of the first coefficient is monotonic, as we should expect in view of the real growth rate predicted in Figure 4, whereas the higher wave numbers exhibit oscillatory growth (Fig. 6) associated with complex growth rates. The results show that the coefficient p_5^c grows only very slowly and that the higher coefficients do not grow significantly, as we should anticipate from Figure 4. The curves for $i > 6$ are omitted for clarity, but no significant growth was observed for wave numbers up to the truncation limit $i = 10$.

Growth of the initially unperturbed wave numbers may be triggered by round-off errors in the computations or by excitation of harmonics of $i = 1$ by nonlinearities as the perturbation passes beyond the linear range. The latter is the more probable mechanism, since double precision was used in the computations and round-off errors would be small. We also note that in the early stages of the process, the most rapidly growing oscillatory perturbations correspond to $i = 3, 4$, whereas Figure 4 indicates that $i = 2, 3$ should have the most rapid growth rates. However, the theoretically predicted behavior becomes dominant at later times. This is consistent with

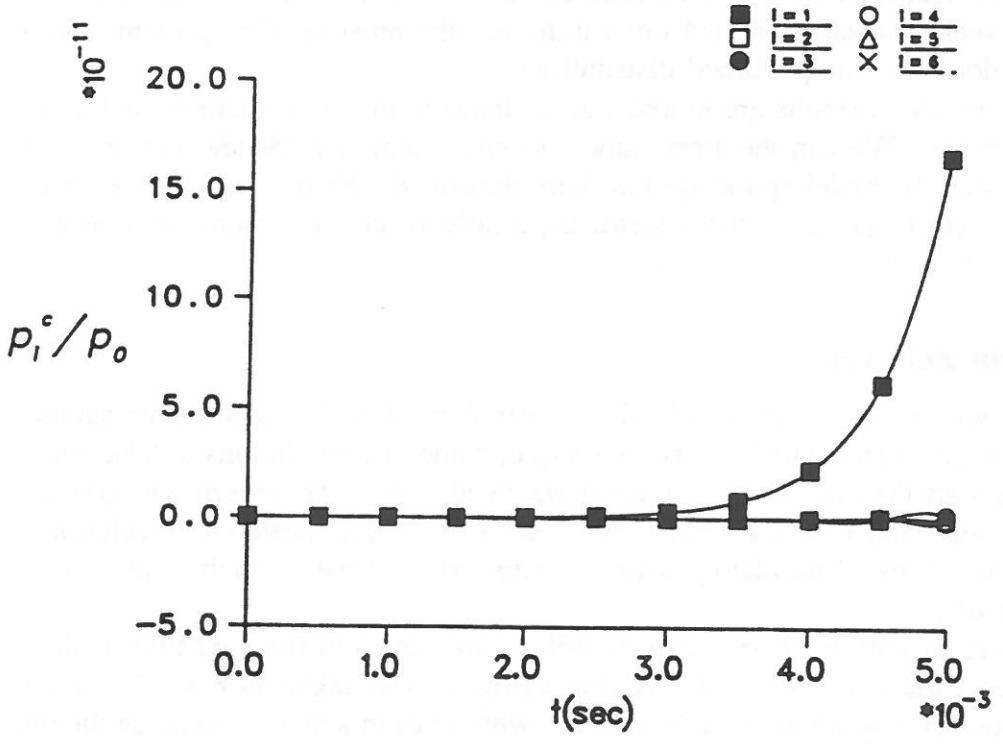

Fig. 5 Growth of the coefficients p_i^c for $i = 1, \ldots, 6$, with $Q^* = -200$.

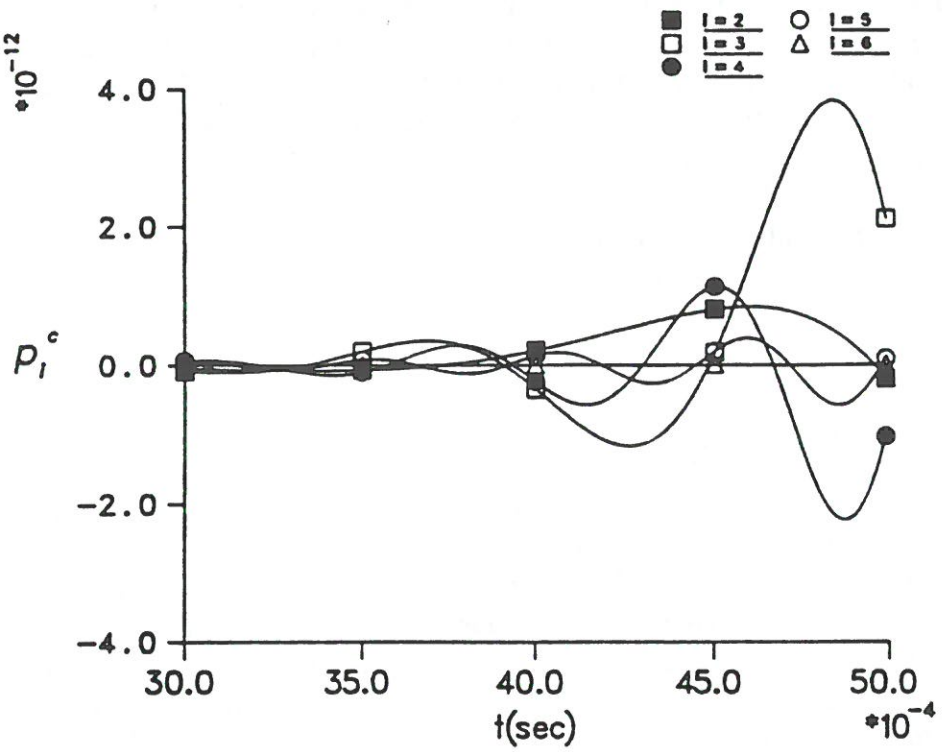

Fig. 6 Enlarged view of Figure 5, showing the oscillatory development of waves with complex growth rates, p_i^c for $i = 2, \ldots, 6$, with $Q^* = -200$.

an excitation mechanism based on nonlinearities—not all coefficients will be equally excited by such a mechanism, but once initiated, the most rapidly growing coefficients will dominate the perturbed distribution.

All of the above results are in exact accordance with the predictions of the two half-plane model. We can therefore conclude with some confidence that the algorithm is accurately modeling the system there described. We next turn our attention to the long-term behavior of the system, especially to the conditions holding after separation first occurs.

Long-Term Behavior

Experience with the two-rod model [6] suggests that when the steady-state solution of a thermoelastic contact problem is nonunique, some of the solutions will be stable. Thus, if we start the system from an *unstable* steady state, the system will gravitate to a stable state and then stay there; however, if a *unique* steady-state solution is unstable, some form of oscillatory behavior must be anticipated, such as that shown in Figure 8 of [6].

Examples of both kinds of behavior will be presented in the next two sections. In both cases, the radius of the contacting cylinders was taken as $r = 25$ mm and the mean contact pressure p_0 to be 0.16 MPa, which lies in a range where the thermal resistance exhibits significant pressure sensitivity.

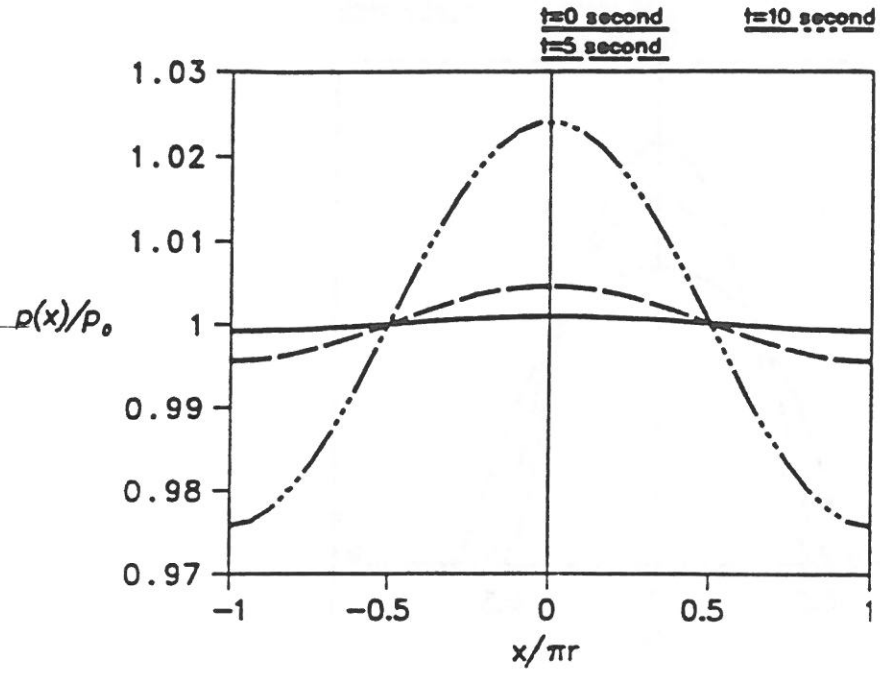

(*a*)

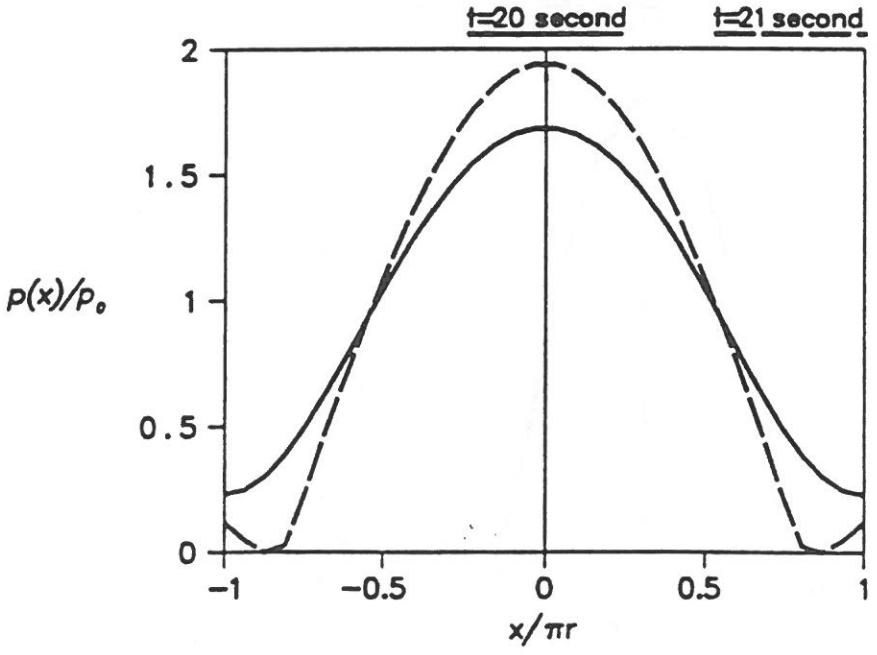

(*b*)

Fig. 7 Development of the pressure distribution for $Q^* = 6$.

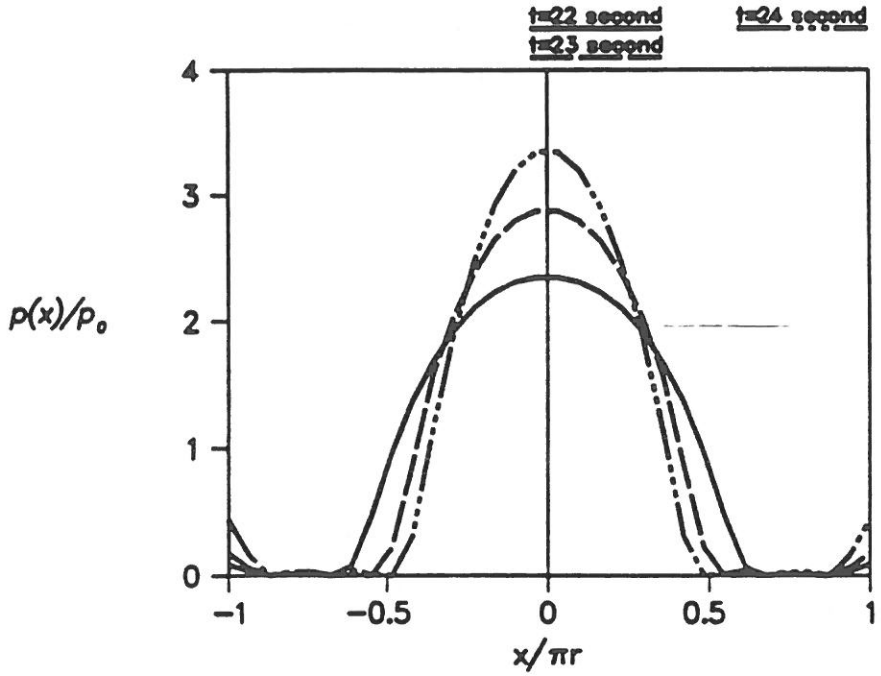

(*c*)

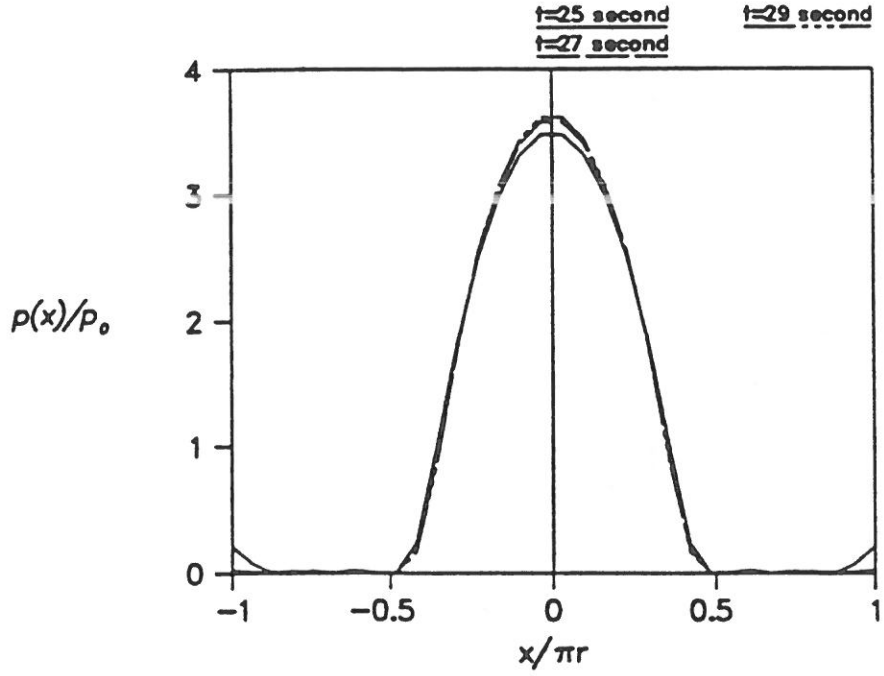

(*d*)

Fig. 7 (Continued)

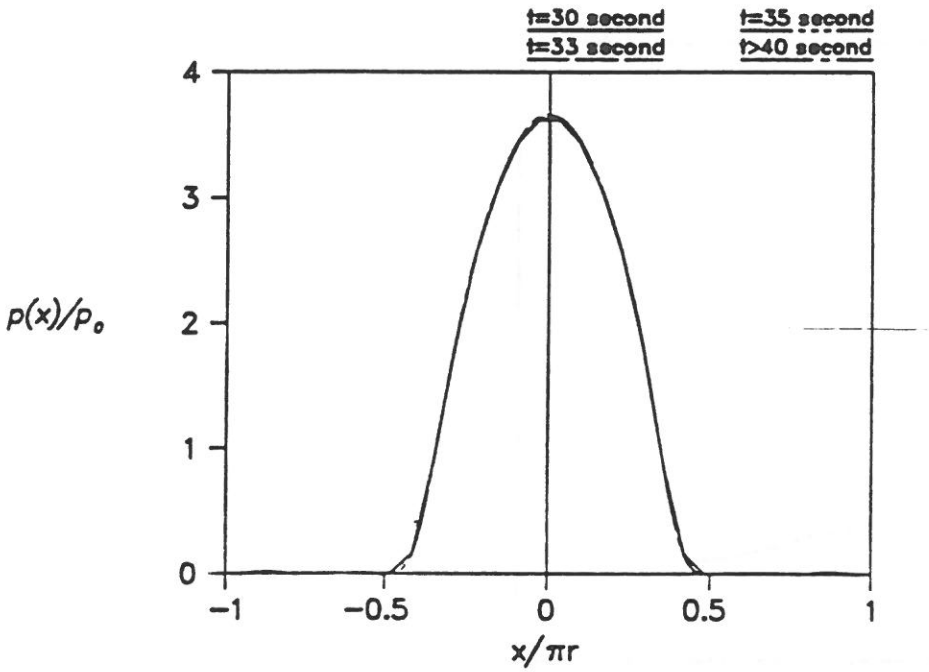

(e)

Fig. 7 (Continued)

Multiple steady states. We expect multiple steady-state solutions when the heat flow is directed into the stainless steel body, since this is the material with the greater distortivity. For this direction of heat flow, the exponential growth rate associated with unstable perturbations is always real (cf. the section on real roots). Figure 7 shows the development of the contact pressure distribution with time for $Q^* = 6$. For this value, only the first harmonic is unstable; hence, the perturbation in contact pressure preserves a sinusoidal form to quite large amplitudes. Separation occurs when $t = 21$ s, after which the pressure distribution converges quite rapidly on a steady state in which there is a central contact region accounting for about 40 percent of the interface.

Qualitatively similar results are obtained at other (positive) values of Q^* in the unstable domain. Generally, increasing Q^* causes the final steady-state contact area to be smaller, as might be anticipated from the solution of the corresponding thermoelastic Hertzian contact problem [17]. Figure 8 shows the relation between Q^* and the proportion c of the interface in contact in the final stable steady state.

Unique unstable steady state. When the heat flux is directed into the aluminium alloy body, which has the lower distortivity, we anticipate that the uniform pressure steady-state solution will be unique. The perturbation analysis [12], however, indicates that for sufficiently large negative Q^* it will be unstable, suggesting some kind of oscillatory long-term behavior.

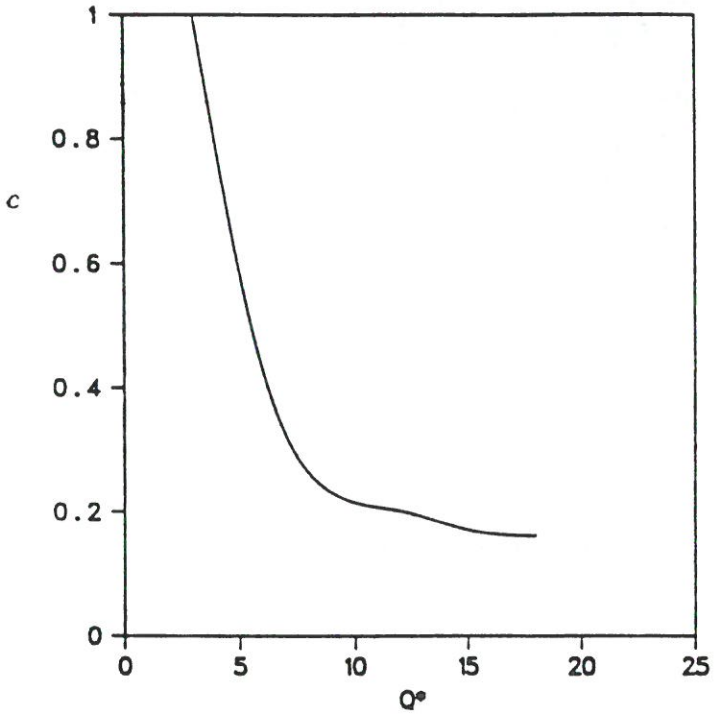

Fig. 8 Proportion of the interface in contact in the final steady state as a function of Q^*, for $Q^* > 0$.

As before, we choose the heat flux ($Q^* = -45$) such that only the first Fourier term is unstable, the corresponding exponential growth rate being complex in this case. The development of the contact pressure distribution is shown in Figure 9. Separation first occurs at $t = 4.1$ s, after which the system alternates between a state with a contact region centered on $x = 0$ and one centered on $x = \pi r$, with a period of approximately 0.27 s. After about $t = 6.5$ s, a different pattern develops in which the pressure distribution and the contact area remain essentially unchanged but move along the interface with constant velocity.

This evolutionary process is illustrated in Figure 10, which shows the extent of the contact area (shaded) as a function of time. The slope of the diagonal bands in the upper part of the figure defines the velocity of the disturbance, which is about 0.58 m/s. The disturbance thus makes one complete circuit of the interface in the same period (0.27 s) as that of the earlier oscillatory phase.

Qualitatively similar behavior is obtained for other values of the parameters, and we conclude that a state with steadily moving contact area and stress and temperature fields is the stable steady state for cases of heat flow into the aluminium alloy body, when the heat flow is sufficient to make the uniform pressure state unstable.

CONCLUSIONS

The principal intention in the present paper has been to develop a simulation of the thermoelastic contact between two thin-walled cylinders, with a view to investigating

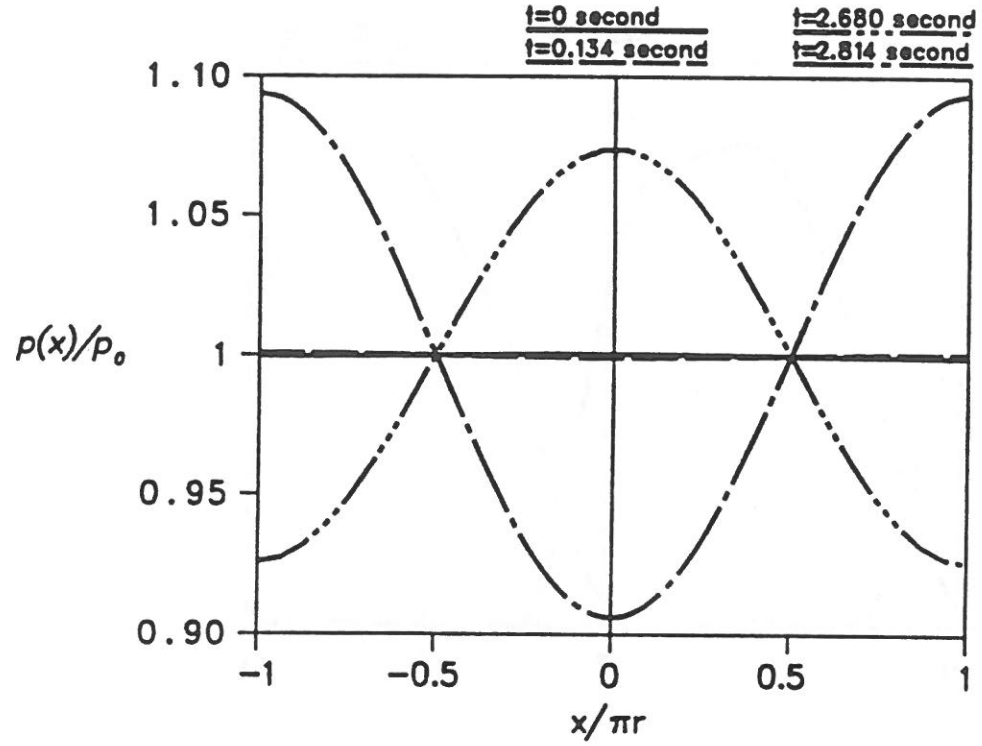

(*a*)

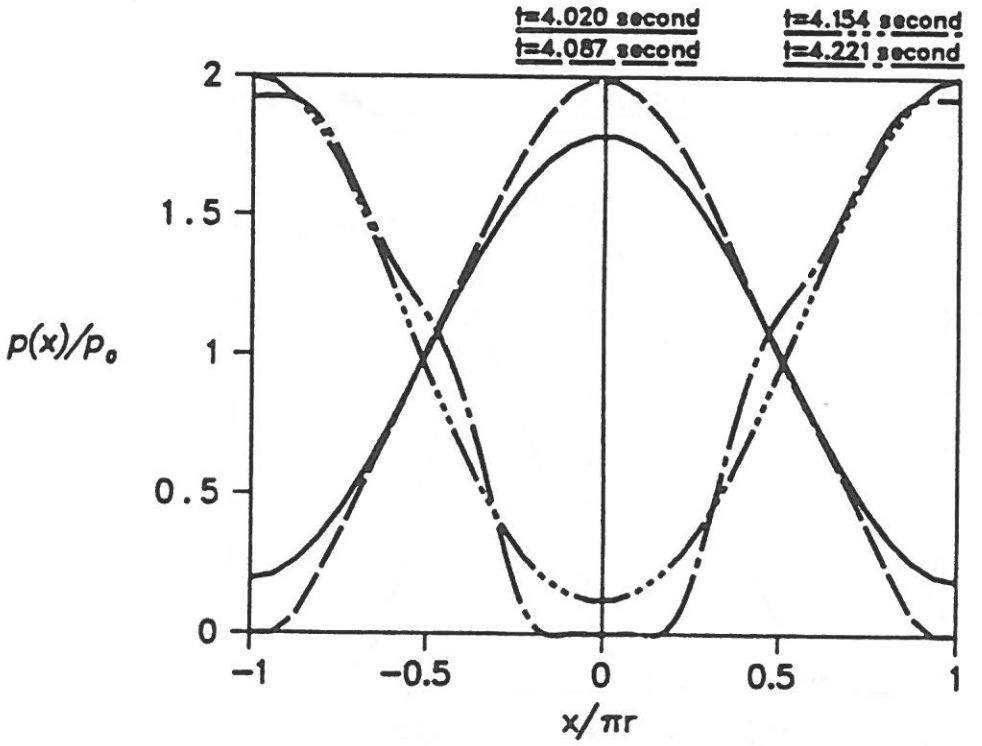

(*b*)

Fig. 9 Development of the pressure distribution for $Q^* = -45$, for which the trivial steady state is unique but unstable.

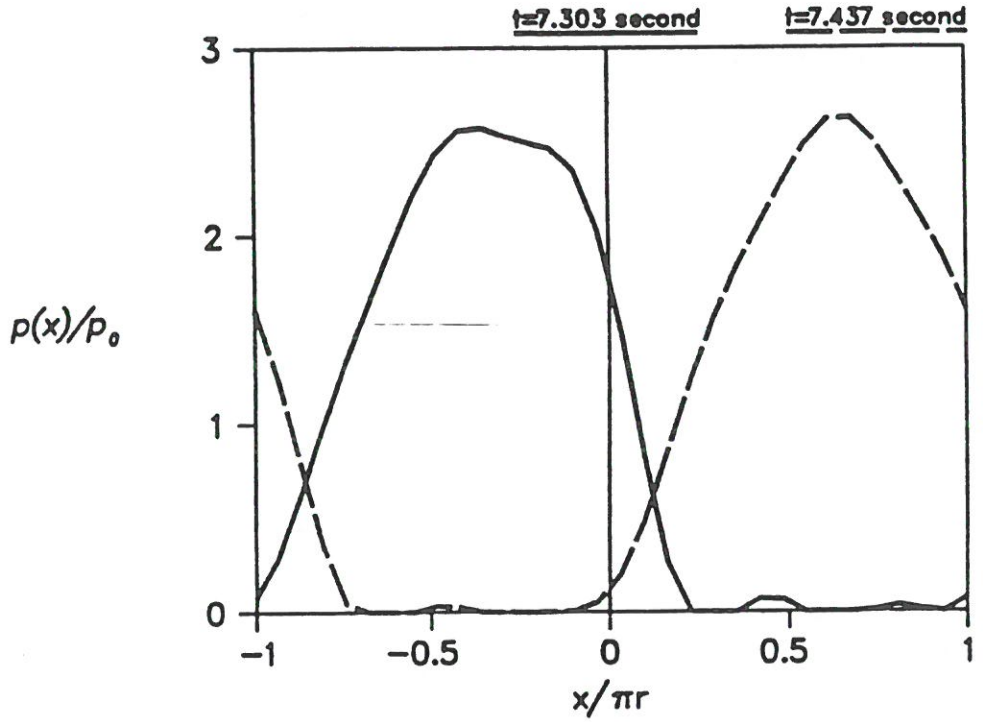

(*c*)

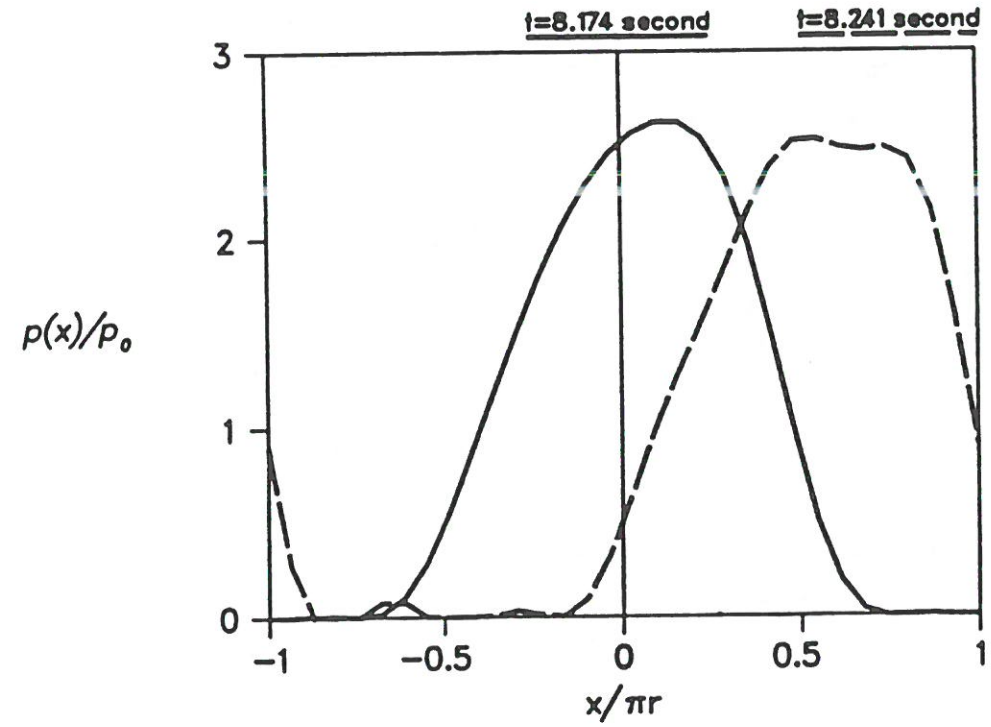

(*d*)

Fig. 9 (Continued)

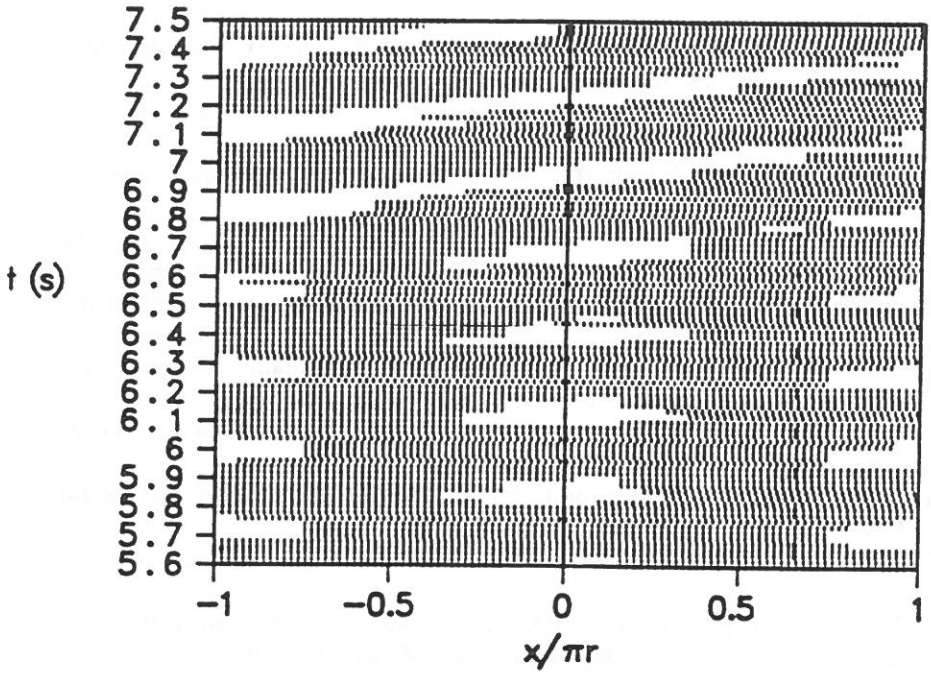

Fig. 10 Extent of the contact area as a function of time for $Q^* = -45$, showing progression from an oscillatory state to one involving a moving contact area.

the behavior of the system after disturbances have grown beyond the linear range treated in earlier perturbation analyses. The results agree with the linear analysis at small values of time, thus confirming the satisfactory operation of the algorithm.

At larger values of time, two categories of behavior are observed, namely,

1. When the heat flows into the more distortive material, the system gravitates to a state with a discrete contact area, which appears to be a stable steady state.
2. When the heat flows into the less distortive material, initially oscillatory behavior is obtained, but eventually the system settles into a state in which the contact area and the stress and temperature fields move around the interface at constant speed while maintaining a constant form.

REFERENCES

1. G. Duvaut, Free Boundary Problem Connected with Thermoelasticity and Unilateral Contact, *Free Boundary Problems*, vol. 11, 1979.
2. P. Shi and M. Shillor, Uniqueness and Stability of the Solution to a Thermoelastic Contact Problem, *Euro. J. Appl. Math.*, vol. 1, pp. 371–387, 1990.
3. J. R. Barber, J. Dundurs, and M. Comninou, Stability Considerations in Thermoelastic Contact, *J. Appl. Mech.*, vol. 47, pp. 871–874, 1980.
4. J. R. Barber, Stability of Thermoelastic Contact for the Aldo Model, *J. Appl. Mech.*, vol. 48, pp. 555–558, 1981.

5. J. R. Barber, Non-Uniqueness and Stability for Heat Conduction Through a Duplex Heat Exchanger Tube, *J. Thermal Stresses*, vol. 9, pp. 69–78, 1986.
6. J. R. Barber and Ronggang Zhang, Transient Behavior and Stability for the Thermoelastic Contact of Two Rods of Dissimilar Materials, *Internat. J. Mech. Sci.*, vol. 30, pp. 691–704, 1988.
7. T. A. Dow and R. A. Burton, Thermoelastic Instability of Sliding Contact in the Absence of Wear, *Wear*, vol. 19, pp. 315–328, 1972.
8. O. Richmond and N. C. Huang, Interface Stability During Unidirectional Solidification of a Pure Metal, *Proc. 6th Canadian Congress of Applied Mechanics, Vancouver*, pp. 453–454, 1977.
9. J. R. Barber, *Stability of Thermoelastic Contact*, Institution of Mechanical Engineers, International Conference on Tribology, Institution of Mechanical Engineers, London, pp. 981–986, 1987.
10. Ronggang Zhang and J. R. Barber, Effect of Material Properties on the Stability of Static Thermoelastic Contact, *J. Appl. Mech.*, vol. 57, pp. 365–369, 1990.
11. T. R. Thomas and S. D. Probert, Thermal Contact Resistance: The Directional Effect and Other Problems, *Internat. J. Heat Mass Transfer*, vol. 13, pp. 789–807, 1970.
12. A. Azarkhin and J. R. Barber, On Partial Contact of a Thin-Walled Circular Cylinder and a Rigid Half-Space, *Internat. J. Mech. Sci.*, vol. 27, pp. 551–557, 1985.
13. H. Carslaw and J. C. Jaeger, *The Conduction of Heat in Solids*, 2nd ed., Clarendon Press, Oxford, 1959.
14. S. P. Timoshenko and J. N. Goodier, *Theory of Elasticity*, 3rd ed., McGraw-Hill, New York, 1970.
15. K. L. Johnson, *Contact Mechanics*, Cambridge University Press, Cambridge, 1985.
16. H. M. Westergaard, Bearing Pressures and Cracks, *J. Appl. Mech.*, vol. 6, pp. 49–53, 1939.
17. J. R. Barber, Indentation of the Semi-Infinite Elastic Solid by a Hot Sphere, *Internat. J. Mech. Sci.*, vol. 15, pp. 813–819, 1973.

Received November 22, 1991